Inorganic Chemistry

Article

pubs.acs.org/IC

Calix[4]arene-Supported Mononuclear Lanthanide Single-Molecule Magnet

Feng Gao,[†,‡] Long Cui,[†] You Song,[†] Yi-Zhi Li,[†] and Jing-Lin Zuo*[,†]

[†]State Key Laboratory of Coordination Chemistry, School of Chemistry and Chemical Engineering, Nanjing National Laboratory of Microstructures, Nanjing University, Hankou Road 9, Nanjing 210093, P. R. China

[‡]School of Chemistry and Chemical Engineering, Jiangsu Key Laboratory of Green Synthetic Chemistry for Functional Materials, Jiangsu Normal University, Shanghai Road 101, Xuzhou 221116, P. R. China

Supporting Information

ABSTRACT: Three new single paramagnetic lanthanide-based complexes, [Ln(L)(L_{OEt})] (Ln^{3+} = Dy^{3+}, Tb^{3+}, and Ho^{3+}), are synthesized with the multidentate calix[4]arene ligand H_2L (H_2L = 5,11,17,23-tetrakis(1,1-dimethylethyl)-25,27-dihydroxy-26,28-dimethoxycalix[4]arene) and Kläui's tripodal ligand L_{OEt}^- (L_{OEt}^- = (η^5-cyclopentadienyl)tris(diethylphosphito-*p*)cobaltate(III)). All of the complexes have been characterized by single crystal X-ray diffraction analysis, thermal stability, absorption spectra, and magnetization measurements. The magnetic properties and magneto-structural correlation in this seven-coordinated system are investigated. The dysprosium complex **1** shows typical single-molecule magnetic behavior with characteristic magnetic hysteresis loops and the slow relaxation of magnetization.

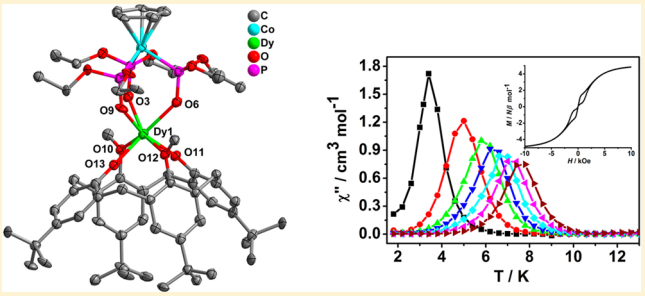

INTRODUCTION

Single-molecule magnets (SMMs) have attracted intensive interest for the last 20 years owing to the intriguing physical properties associated with the quantum tunneling of magnetization (QTM)[1] and potential applications in magnetic storage, sensors, and nanoscale electronic devices.[2] Recently, particular emphasis has been placed on the design of SMMs with lanthanide ions due to the significant magnetic anisotropy arising from the large, unquenched orbital angular momentum.[3] Among them, the mononuclear system in which single lanthanide ion lies in an effective crystal field can also exhibit typically slow relaxation of the magnetization. This family, known as single lanthanide-based molecular magnets, has rapidly developed and provides the important implication that the interaction between the anisotropy of the paramagnetic ion and the ligand field environment plays a crucial role in tuning their magnetic properties.[3a,e,4,5]

One of the effective synthetic strategies for isolating small and simple SMMs, the magnetic skeleton being completely encapsulated within a rigid organic or inorganic sheath, may control the intermolecular dipolar interactions, therefore simplifying the analysis of local anisotropy. As a representative, calix[4]arene and its derivatives are typically bowl-shaped macrocyclic molecules which have been exploited in the construction of various polynuclear architectures. Their rigid conformations can be utilized to present multidentate coordination sites for assembly directing metal cores, rendering them good ligand candidates for the isolation of paramagnetic metal ions in high-symmetry coordination geometry.[6,7]

To our knowledge, no calix[4]arene-supported single Ln(III)-based SMMs were reported in the literature. Herein, for the first time, three new lanthanide complexes with the general formula [Ln(L)(L_{OEt})] [Ln^{3+} = Dy^{3+} (**1**), Tb^{3+} (**2**), and Ho^{3+} (**3**)] are synthesized on the basis of multidentate calix[4]arene ligand H_2L (H_2L = 5,11,17,23-tetrakis(1,1-dimethylethyl)-25,27-dihydroxy-26,28-dimethoxycalix[4]arene) and Kläui's tripodal ligand NaL_{OEt} (NaL_{OEt} = sodium (η^5-cyclopentadienyl)tris(diethylphosphito-*p*)cobaltate(III)). These complexes were structurally characterized, and their static and dynamic magnetic properties were investigated. Interestingly, the dysprosium complex **1** behaves as a SMM with magnetic hysteresis loops and the slow relaxation of magnetization.

EXPERIMENTAL SECTION

General Information. All chemicals and solvents were obtained and used directly from the commercial sources. Starting materials, calix[4]arene ligand H_2L and Kläui's ligand NaL_{OEt}, were prepared according to the published methods.[8,9] Elemental analysis was carried out with a Elementar Vario MICRO analyzer. IR spectra were recorded on a Vector22 Bruker spectrophotometer with KBr pellets. Melting points were determined with X-4 digital micro melting point apparatus. UV−vis spectra were obtained with a UV-3600 spectrophotometer. TGA curves were obtained on a STA 449 F3 Jupiter thermal analyzer.

Received: October 23, 2013
Published: December 19, 2013

Table 1. Crystallographic Data for Complexes 1, 2, and 3

	1	2	3
formula	$C_{63}H_{93}CoDyO_{13}P_3$	$C_{63}H_{93}CoTbO_{13}P_3$	$C_{63}H_{93}CoHoO_{13}P_3$
fw	1372.71	1369.13	1375.14
cryst syst	triclinic	triclinic	triclinic
space group	$P\bar{1}$	$P\bar{1}$	$P\bar{1}$
a, Å	10.9895(10)	10.9869(12)	11.1053(8)
b, Å	16.0209(15)	16.0612(17)	16.0939(11)
c, Å	19.9307(18)	19.974(2)	20.2194(14)
α, deg	99.4430(10)	99.4630(10)	99.4640(10)
β, deg	101.6260(10)	101.538(2)	101.065(2)
γ, deg	102.1450(10)	102.0990(10)	101.9110(10)
V, Å^3	3281.1(5)	3297.5(6)	3391.0(4)
Z	2	2	2
ρ_{calcd}, g cm^{-3}	1.389	1.379	1.347
T/K	123(2)	123(2)	123(2)
μ, mm^{-1}	1.514	1.446	1.530
θ, deg	1.07−26.00	1.33−26.00	1.05−26.00
F(000)	1426	1424	1428
index ranges	$-13 \le h \le 13$, $-19 \le k \le 19$, $-24 \le l \le 20$	$-13 \le h \le 13$, $-19 \le k \le 19$, $-24 \le l \le 19$	$-12 \le h \le 13$, $-19 \le k \le 19$, $-23 \le l \le 24$
data/ restraints/ params	12 741/0/749	12 801/0/749	13 262/0/749
GOF (F^2)	1.058	1.052	1.068
R1,[a] wR2[b] ($I > 2\sigma(I)$)	0.0596, 0.1501	0.0567, 0.1439	0.0604, 0.1518
R1,[a] wR$_2$[b] (all data)	0.0614, 0.1509	0.0583, 0.1445	0.0654, 0.1529

[a] $R1 = \Sigma||F_o| - |F_c||/\Sigma|F_o|$. [b] $wR2 = [\Sigma w(F_o^2 - F_c^2)^2/\Sigma w(F_o^2)^2]^{1/2}$.

X-ray Crystallography. The crystal structures were determined at 123 K on a Bruker SMART CCD diffractometer using monochromated Mo Kα radiation (λ = 0.710 73 Å). The cell parameters were retrieved using SMART software and refined using SAINT[10] for all observed reflections. The data were collected using a narrow-frame method with scan widths of 0.30° in ω and an exposure time of 5 s/frame. The redundant data sets were reduced using SAINT[10] and corrected both for Lorentz and polarization effects. The absorption corrections were applied using SADABS[11] supplied by Bruker. The structures were solved and refined using the program SHELXL-97.[12] Direct method yielded all non-hydrogen atoms, which were refined with anisotropic thermal parameters. All hydrogen atom positions were calculated geometrically and were riding on their respective atoms. More details for the data collections and structure refinements were given in Table 1. The selected bond lengths and bond angles were listed in Table 2 [CCDC reference numbers 966636 (**1**), 966637 (**2**), 966638 (**3**)].

Magnetic Measurement. Magnetic susceptibility measurements for polycrystalline sample were performed on a Quantum Design MPMS-SQUID-VSM magnetometer between 1.8 and 300 K for direct current (dc) applied fields ranging from 0 to 70 kOe. Alternating current (ac) susceptibilities were obtained under oscillating ac field of 2 Oe and in the frequency range 1−999 Hz. Diamagnetic corrections were calculated using Pascal's constants,[13] and an experimental correction for the diamagnetic sample holder was applied.

*Synthesis of [Dy(L)(L$_{OEt}$)] (**1**).* The calix[4]arene ligand H_2L (13.5 mg, 0.02 mmol), NaL_{OEt} (11.5 mg, 0.02 mmol), and $Dy(acac)_3{\cdot}2H_2O$ (9.2 mg, 0.02 mmol) were dissolved in 10 mL of acetone/methanol (1:1 v/v). The reaction mixture was stirred and heated at 85 °C for 6 h, and then cooled to the room temperature. Yellow block-shaped crystals of **1** were obtained and collected by filtration after slow evaporation of mother liquid for several days. Yield = 58%. Mp > 300 °C. Anal. Calcd for $C_{63}H_{93}CoDyO_{13}P_3$: C, 55.12; H, 6.83. Found: C, 55.35; H, 7.08. Selected IR (KBr, cm^{-1}): 2960(s), 2900(m), 1601(w), 1482(s), 1360(m), 1141(s), 1021(m), 933(s), 838(m), 769(m), 594(s). UV−vis {(CH_2Cl_2, λmax/nm, [log (ε/dm^3 mol^{-1} cm^{-1})] in parentheses}: 242(4.65), 312(3.96), 339(3.47).

Table 2. Selected Bond Lengths (Å) and Bond Angles (deg) for complexes 1, 2, and 3

	1	2	3
	Bond Distances (Å)		
Ln1−O3	2.295(3)	2.299(2)	2.287(3)
Ln1−O6	2.330(3)	2.343(2)	2.336(3)
Ln1−O9	2.321(3)	2.349(2)	2.319(3)
Ln1−O10	2.678(3)	2.680(3)	2.709(3)
Ln1−O11	2.122(3)	2.134(3)	2.132(3)
Ln1−O12	2.493(3)	2.497(2)	2.477(3)
Ln1−O13	2.131(3)	2.144(2)	2.127(3)
	Bond Angles (deg)		
O3−Ln1−O6	80.03(10)	78.28(9)	79.92(12)
O6−Ln1−O9	77.02(10)	76.88(9)	76.77(12)
O3−Ln1−O9	78.45(11)	79.93(9)	78.77(13)
O3−Ln1−O10	68.74(9)	69.29(8)	68.28(11)
O3−Ln1−O11	112.89(11)	118.64(10)	111.49(13)
O3−Ln1−O12	150.42(10)	150.38(9)	150.85(12)
O3−Ln1−O13	118.19(10)	112.91(10)	118.94(13)
O6−Ln1−O10	133.68(10)	126.04(8)	133.99(11)
O6−Ln1−O11	86.01(10)	84.45(10)	86.54(13)
O6−Ln1−O12	75.68(10)	79.93(8)	75.44(12)
O6−Ln1−O13	150.73(11)	157.68(10)	151.03(13)
O9−Ln1−O10	125.88(10)	134.08(8)	125.31(12)
O9−Ln1−O11	157.81(12)	150.47(10)	158.75(14)
O9−Ln1−O12	79.85(10)	75.76(9)	80.62(12)
O9−Ln1−O13	84.24(10)	85.93(9)	85.28(12)
O10−Ln1−O11	76.27(10)	75.45(9)	75.85(12)
O10−Ln1−O12	140.84(9)	140.32(8)	140.86(11)
O10−Ln1−O13	75.58(10)	76.24(9)	74.98(12)
O11−Ln1−O12	82.18(10)	78.62(9)	82.53(12)
O11−Ln1−O13	105.03(11)	104.93(10)	104.23(13)
O12−Ln1−O13	79.06(10)	82.14(9)	79.36(12)

dx.doi.org/10.1021/ic4026624 | Inorg. Chem. 2014, 53, 562−567

*Synthesis of [Tb(L)(L$_{OEt}$)] (**2**).* The procedure was similar to the synthesis of **1** except that Tb(acac)$_3$·2H$_2$O was used in place of Dy(acac)$_3$·2H$_2$O. The resultant yellow block-shaped crystals of **2** were obtained and collected. Yield = 55%. Mp > 300 °C. Anal. Calcd for $C_{63}H_{93}CoTbO_{13}P_3$: C, 55.26; H, 6.85. Found: C, 55.49; H, 7.11. Selected IR (KBr, cm^{-1}): 2960(s), 2900(m), 1602(w), 1482(s), 1361(m), 1140(s), 1020(m), 935(s), 837(m), 770(m), 595(s). UV–vis {(CH$_2$Cl$_2$, λ_{max}/nm, [log (ε/dm^3 mol^{-1} cm^{-1})] in parentheses}: 243(4.67), 311(3.98), 339(3.50).

*Synthesis of [Ho(L)(L$_{OEt}$)] (**3**).* The procedure was similar to the synthesis of **1** except that Ho(acac)$_3$·2H$_2$O was used in place of Dy(acac)$_3$·2H$_2$O. The resultant yellow block-shaped crystals of **3** were obtained and collected. Yield = 56%. Mp > 300 °C. Anal. Calcd for $C_{63}H_{93}CoHoO_{13}P_3$: C, 55.02; H, 6.82. Found: C, 55.26; H, 7.05. Selected IR (KBr, cm^{-1}): 2961(s), 2901(m), 1601(w), 1483(s), 1361(m), 1141(s), 1022(m), 934(s), 838(m), 769(m), 596(s). UV–vis {(CH$_2$Cl$_2$, λ_{max}/nm, [log (ε/dm^3 mol^{-1} cm^{-1})] in parentheses}: 242(4.68), 313(4.00), 338(3.51).

RESULTS AND DISCUSSION

Synthesis and Characterization. Reaction of lanthanide acetylacetonate, calix[4]arene ligand H$_2$L, and Kläui's tripodal ligand NaL$_{OEt}$ in a 1:1:1 molar ratio in methanol and acetone resulted into the formation of target complexes (Scheme 1).

Scheme 1. Synthesis of Complexes [Ln(L)(L$_{OEt}$)] [Ln^{3+} = Dy^{3+} (1), Tb^{3+} (2), and Ho^{3+} (3)]

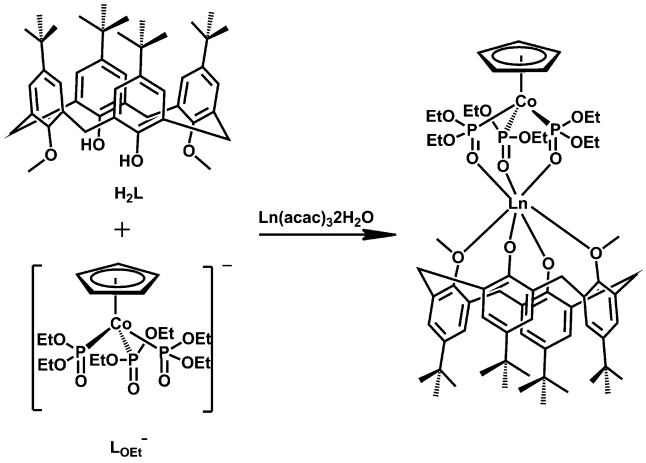

Perfect yellow block-shaped crystals were obtained after slow evaporation of the mother liquor. These complexes are very soluble in common organic solvents, and more importantly, they are quite thermally stable in the solid state with the decomposition starting beyond 350 °C (Figure S1, Supporting Information). More characterization has been performed by elemental analysis, IR, UV–vis absorption spectra (Figure S2, Supporting Information), and X-ray single crystal diffraction analysis.

Crystal Structural Description. Single crystal X-ray analysis reveals that all of the complexes are isomorphous and crystallize in the triclinic space group $P\bar{1}$. As shown in Figure 1, the molecule contains a seven-coordinated paramagnetic Ln(III) ion [Ln^{3+} = Dy^{3+} (**1**), Tb^{3+} (**2**), and Ho^{3+} (**3**)], bonded to three O atoms from L$_{OEt}^-$ and four O atoms from L^{2-}. The anionic L$_{OEt}^-$ ligand caps on the lanthanide ion, in which the Co(III) ion is surrounded by cyclopentadienyl ring and three P atoms. The distance for Co^{3+}···Ln^{3+} is 4.288(7), 4.299(6), and 4.286(7) Å for **1**, **2**, and **3**, respectively. The Ln(III)–O bond lengths range from 2.122(3) to 2.678(3) Å for

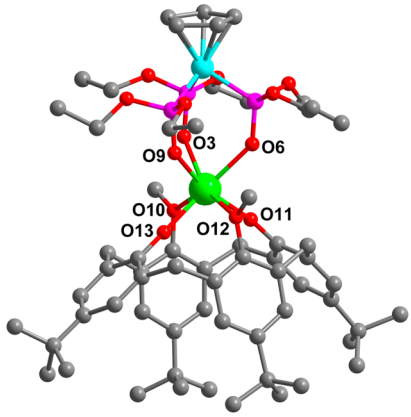

Figure 1. Crystal structure of complexes [Ln(L)(L$_{OEt}$)] [Ln^{3+} = Dy^{3+} (**1**), Tb^{3+} (**2**), and Ho^{3+} (**3**)]. H atoms are omitted for clarity (Ln green, Co blue, P purple, O red, and C gray).

1, 2.134(3) to 2.680(3) Å for **2**, and 2.127(3) to 2.709(3) Å for **3**, with the average distance of 2.338, 2.349, and 2.341 Å for **1**, **2**, and **3**, respectively. The dihedral angle between O10O11O13 and O12O11O13 planes is 19.84(12)° for **1**, 19.72(9)° for **2**, and 20.27(11)° for **3**, indicating the nonplanarity of four oxygen atoms in the calix[4]arene ligand. The two planes between cyclopentadienyl ring and O3O6O9 of the phosphito groups in L$_{OEt}^-$ ligand are almost parallel to each other with the angle of 0.89(12)° for **1**, 0.94(13)° for **2**, and 1.01(12)° for **3**. Furthermore, the extended structure (Figure 2), constructed by

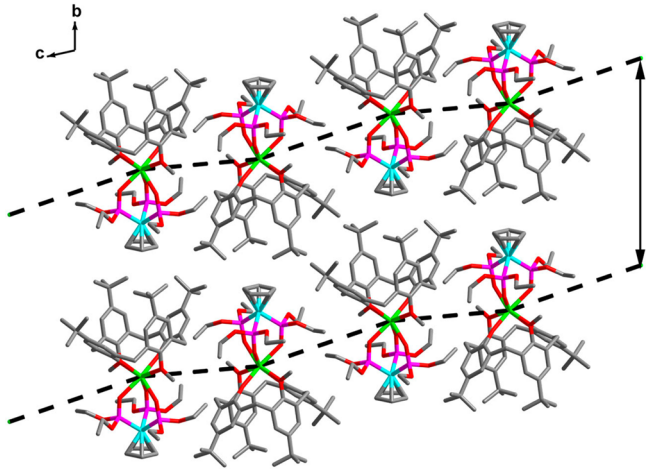

Figure 2. Extended structure of complexes [Ln(L)(L$_{OEt}$)] [Ln^{3+} = Dy^{3+} (**1**), Tb^{3+} (**2**), and Ho^{3+} (**3**)] showing zigzig layer array with separation indicated by an arrow. H atoms are omitted for clarity.

the head-to-tail stacking of the coordination units, shows zigzig layers in an array with a separation of 16.021(2) Å for **1**, 16.061(2) Å for **2**, and 16.094(2) Å for **3**, and the shortest intermolecular distance for Ln^{3+}···Ln^{3+} is 10.325(2), 10.316(2), and 10.415(1) Å for **1**, **2**, and **3**, respectively. All of the results indicate that the two sterically bulky ligands provide a compact environment around the lanthanide core, resulting into the effective isolation of entire molecule.

Static Magnetic Properties. Direct current magnetic susceptibility data for all of the complexes were collected in the temperature range 1.8–300 K under an applied magnetic field of 1 kOe. As shown in Figure 3, the temperature dependence of the magnetic susceptibility provides the

dx.doi.org/10.1021/ic4026624 | Inorg. Chem. 2014, 53, 562–567

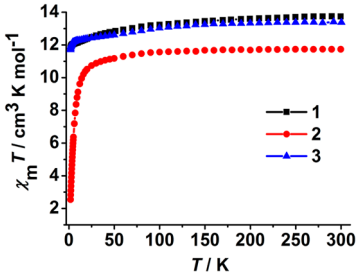

Figure 3. $\chi_M T$ versus T plots for **1**, **2**, and **3** under 1 kOe dc field.

following $\chi_M T$ values at room temperature, 13.74 cm^3 K mol^{-1} for **1**, 11.73 cm^3 K mol^{-1} for **2**, and 13.40 cm^3 K mol^{-1} for **3**, which are close to the expected value for one uncoupled Ln(III) ion (14.17 cm^3 K mol^{-1} for Dy(III), $^6H_{15/2}$, $S = {}^5/_2$, $L = 5$, $g = {}^4/_3$, $J = {}^{15}/_2$; 11.82 cm^3 K mol^{-1} for Tb(III), $^7F_6$, $S = 3$, $L = 3$, $J = 6$, $g = {}^3/_2$; 14.07 cm^3 K mol^{-1} for Ho(III), $^5I_8$, $S = 2$, $L = 6$, $J = 8$, $g = {}^5/_4$). With lowering temperature, the observed $\chi_M T$ product gradually decreases, and then drops to a minimum value of 11.78, 2.55, and 11.70 cm^3 K mol^{-1} for **1**, **2**, and **3**, respectively, at 1.8 K as a consequence of the depopulation of sublevels of the ground J multiplet split by the crystal field[4f,14] and/or possible intermolecular antiferromagnetic interactions.[14a]

Field-dependent magnetization for all of the complexes at 1.8 K rapidly increases at lower magnetic fields, and then slowly reaches a maximum value at 70 kOe (5.34 Nβ for **1**, 4.91 Nβ for **2**, and 5.19 Nβ for **3**) (Figure 4). They are smaller than the

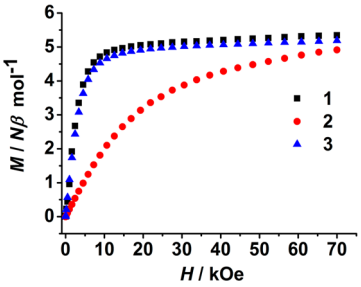

Figure 4. M versus H plots for **1**, **2**, and **3** at 1.8 K with a sweeping rate of 500 Oe s^{-1}.

theoretical saturation value for a single Ln(III) ion (10 Nβ for Dy, 9 Nβ for Tb, and 10 Nβ for Ho), likely due to the existence of crystal-field effects and low-lying excited states.[5h,15,16] The hysteresis loops were further recorded for the powder samples of **1**–**3**. No obvious hysteresis loops were observed for complexes **2** and **3** (Figures S3 and S4, Supporting Information), while a small butterfly shaped loop for complex **1** can be found at 1.8 K as plotted in Figure 5. Furthermore, the coercive field of these loops for **1** increases upon cooling, and exhibits strong sweep-rate dependence (Figure S5, Supporting Information), suggesting the presence of QTM that the tunneling can be diminished as the field sweeping rate is increased.[17]

Dynamic Magnetic Properties. Alternating current susceptibility measurements were carried out for all of the complexes to investigate the slow relaxation of the magnetization. For Dy complex **1**, both the temperature- and frequency-dependent ac susceptibilities display obvious in-phase (χ') and out-of-phase (χ'') signals under $H_{dc} = 0$ Oe and $H_{ac} = 2$ Oe, but the presence of strong QTM results in the

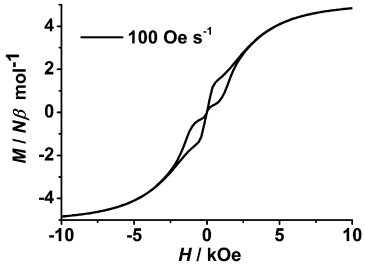

Figure 5. Hysteresis loop for **1** at 1.8 K with a sweeping rate of 100 Oe s^{-1}.

observation that no maxima of χ'' signals can be found above 1.8 K (Figures S6 and S7, Supporting Information). Such behavior is often reported in Ln-SMMs.[4a,c,5c,f,18] In order to effectively suppress QTM, a small dc field of 900 Oe is applied, and the well-shaped peaks of χ'' signal can be fully observed at frequencies as low as 1 Hz (Figure 6a). The anisotropic energy barrier (Δ/k_B) of 73.7 K can be estimated according to the Arrhenius law [$\tau = \tau_0 \exp(\Delta/k_B T)$] with the pre-exponential factor $\tau_0 = 9.1 \times 10^{-9}$ s ($R = 0.9974$) (Figure 6b), confirming a field-induced SMM behavior.

For complexes **2** and **3**, no obvious χ'' susceptibility signals were observed at the high frequency of 999 Hz from 13.0 to 1.8 K under both zero dc field and the same external dc field of 900 Oe (Figures S8–S11, Supporting Information), which likely attributed to their non-Kramers' system [even number of f-electrons for Tb(III) and Ho(III)] behaving as a non-degenerate ground state with larger energy gaps between the lowest excited state and ground state.[5h,19]

To further probe the dynamics of magnetization for **1**, variable-frequency ac susceptibilities were also measured under 900 Oe dc field in the temperature range 3.0–8.0 K (Figure 7a). The peaks for χ'' signal exhibit gradual transition toward the low-frequency region with decreasing temperature down to 3.0 K, and symmetrically semicircular shapes can be well presented in the corresponding Cole–Cole plots (Figure 7b). Through fitting the data with a generalized Debye model[20] from 4.0 to 7.0 K, the parameter α can be obtained in the range 0.022–0.035 (Table S1, Supporting Information), indicating an obviously single relaxation process in this system.

In our previous work, some similar dysprosium complexes supported by different type of macrocyclic ligands, such as Schiff base ligand, porphyrin (TPP), and phthalocyanine (Pc), have been synthesized to study magnetostructural correlation in the "4:3 piano stool" seven-coordinated system.[5f–h] The Dy(III) complex **1** displays obvious temperature- and frequency-dependent ac signals under a smaller static field and a higher energy barrier (73.7 K), in comparison with 8.5 K for [Dy(TPP)(L_{OEt})],[5f] 23.6 K for [Dy(Pc)(L_{OEt})],[5f] 41.6 K for [Dy(TTF-Schffibase)(L_{OEt})],[5h] and 24.61 K for [Dy(salphen)-(L_{OEt})].[5g] Consequently, a slight structural modification leads to the influence on the local coordination environment and nature of 4f ion anisotropy, which may generate the different SMM behavior.[5a,i,j] In the present system, polyphenoxy moieties of the calix[4]arene ligand and phosphito groups of Kläui's tripodal ligand were investigated for their strong coordination ability toward lanthanide(III) ions (the higher affinity between Ln^{3+} ion and O atoms over Ln^{3+} ion and N atoms from Schiff base ligand, TPP and Pc). Additionally, the shortest intermolecular $Dy^{3+}\cdots Dy^{3+}$ distance (10.325 Å for **1**) is also longer than that of our previously reported Dy-SMMs,

dx.doi.org/10.1021/ic4026624 | Inorg. Chem. 2014, 53, 562–567

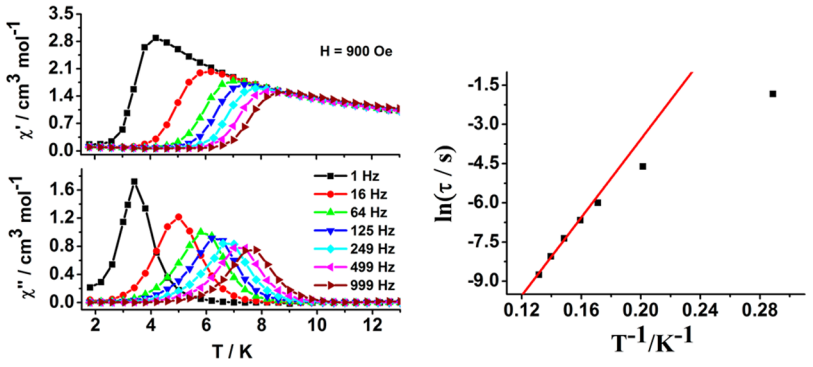

(a) (b)

Figure 6. (a) Temperature-dependent in-phase (χ') and out-of-phase (χ'') ac susceptibility signals at the indicated frequencies (1–999 Hz) for **1** under 900 Oe dc field. Solid lines are only guides for the eye; (b) ln τ versus T^{-1} plots for **1**. Red line represents the best fit to the Arrhenius law.

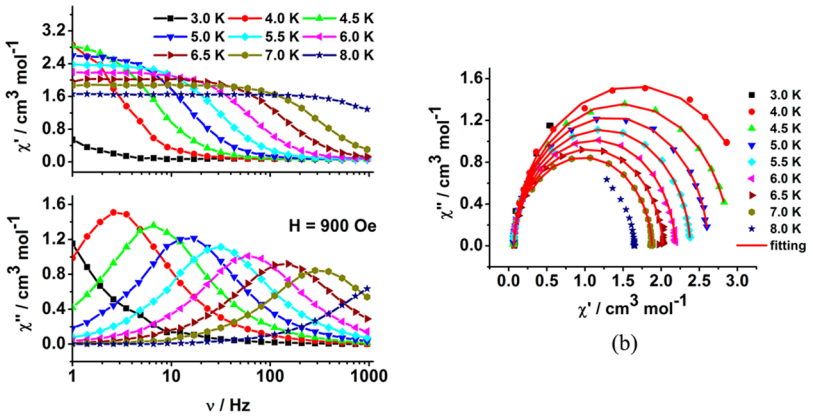

(a) (b)

Figure 7. (a) Frequency-dependent in-phase (χ') and out-of-phase (χ'') ac susceptibility signals for **1** at the indicated temperature (3.0–8.0 K) under 900 Oe dc field. Solid lines are only guides for the eye; (b) Cole–Cole plots for **1**. Red lines represent the fit to the general Debye model.

indicating that the rigid conformation of ligands with large steric hindrance affords a "protective" shealth for isolated molecule magnets and weakens intermolecular f–f interactions. The results further confirm that this type of single lanthanide-based SMM feature is closely related to the intrinsic molecular properties, such as lanthanide ion anisotropy, intermolecular dipolar interactions, ligand field strength, and crystal field symmetry.

CONCLUSIONS

A new family of single lanthanide-based complexes supported by macrocyclic multidentate calix[4]arene ligand were successfully isolated and structurally characterized. Static and dynamic susceptibility measurements were made for all of the complexes. The dysprosium complex displays obvious SMM behavior with higher anisotropic energy barrier and characteristic magnetic hysteresis loops. The introduction of bulky calix[4]arene and Kläui's tripodal ligands may effectively encapsulate the paramagnetic lanthanide ion, thereby shielding it from interactions with the environment. This work provides further possibilities for controlling self-assembly and tuning of the magnetic properties for lanthanide complexes, and more works on similar systems are underway in our laboratory.

ASSOCIATED CONTENT

Supporting Information

Supplementary table and figures, and additional characterization and X-ray crystallographic files in CIF format for **1**–**3**. This material is available free of charge via the Internet at http://pubs.acs.org.

AUTHOR INFORMATION

Corresponding Author

*E-mail: zuojl@nju.edu.cn. Fax: +86-25-83314502.

Notes

The authors declare no competing financial interest.

ACKNOWLEDGMENTS

This work was supported by the Major State Basic Research Development Program (2013CB922100 and 2011CB808704), and the National Natural Science Foundation of China (91022031 and 51173075). We also thank Dr. Tian-Wei Wang for experimental assistance on magnetic measurements.

REFERENCES

(1) (a) Gatteschi, D.; Sessoli, R.; Villain, J. *Molecular Nanomagnets*; Oxford University Press: New York, 2006. (b) Gatteschi, D.; Sessoli, R. *Angew. Chem., Int. Ed.* **2003**, *42*, 268.

(2) (a) Leuenberger, M. N.; Loss, D. *Nature* **2001**, *410*, 789. (b) Saitoh, E.; Miyajima, H.; Yamaoka, T.; Tatara, G. *Nature* **2004**,

432, 203. (c) Bogani, L.; Wernsdorfer, W. *Nat. Mater.* **2008**, *7*, 179. (d) Troiani, F.; Affronte, M. *Chem. Soc. Rev.* **2011**, *40*, 3119. (e) Sessoli, R.; Gatteschi, D.; Caneschi, A.; Novak, M. A. *Nature* **1993**, *365*, 141.

(3) (a) Woodruff, D. N.; Winpenny, R. E. P.; Layfield, R. A. *Chem. Rev.* **2013**, *113*, 5110. (b) Katoh, K.; Isshiki, H.; Komeda, T.; Yamashita, M. *Coord. Chem. Rev.* **2011**, *255*, 2124. (c) Murugesu, M.; Habib, F. *Chem. Soc. Rev.* **2013**, *42*, 3278. (d) Sessoli, R.; Powell, A. K. *Coord. Chem. Rev.* **2009**, *253*, 2328. (e) Zhang, P.; Guo, Y.-N.; Tang, J.-K. *Coord. Chem. Rev.* **2013**, *257*, 1728. (f) Guo, Y.-N.; Xu, G.-F.; Gamez, P.; Zhao, L.; Lin, S.-Y.; Deng, R.-P.; Tang, J.-K.; Zhang, H.-J. *J. Am. Chem. Soc.* **2010**, *132*, 8538. (g) Guo, Y.-N.; Xu, G.-F.; Wernsdorfer, W.; Ungur, L.; Guo, Y.; Tang, J.-K.; Zhang, H.-J.; Chibotaru, L. F.; Powell, A. K. *J. Am. Chem. Soc.* **2011**, *133*, 11948. (h) Lin, S.-Y.; Wernsdorfer, W.; Ungur, L.; Powell, A. K.; Guo, Y.-N.; Tang, J.-K.; Zhao, L.; Chibotaru, L. F.; Zhang, H.-J. *Angew. Chem., Int. Ed.* **2012**, *51*, 12767.

(4) (a) Ishikawa, N.; Mizuno, Y.; Takamatsu, S.; Ishikawa, T.; Koshihara, S. *Inorg. Chem.* **2008**, *47*, 10217. (b) AlDamen, M. A.; Clemente-Juan, J. M.; Coronado, E.; Marti-Gastaldo, C.; Gaita-Arino, A. *J. Am. Chem. Soc.* **2008**, *130*, 8874. (c) Wang, H.-L.; Wang, K.; Tao, J.; Jiang, J.-Z. *Chem. Commun.* **2012**, *48*, 2973. (d) Chen, G.-J.; Guo, Y.-N.; Tian, J.-L.; Tang, J.-K.; Gu, W.; Liu, X.; Yan, S.-P.; Cheng, P.; Liao, D.-Z. *Chem.—Eur. J.* **2012**, *18*, 2484. (e) Chilton, N. F.; Langley, S. K.; Moubaraki, B.; Soncini, A.; Batten, S. R.; Murray, K. S. *Chem. Sci.* **2013**, *4*, 1719. (f) Wang, Y.-L.; Ma, Y.; Yang, X.; Tang, J.-K.; Cheng, P.; Wang, Q.-L.; Li, L.-C.; Liao, D.-Z. *Inorg. Chem.* **2013**, *52*, 7380. (g) Ren, M.; Pinkowicz, D.; Yoon, M.; Kim, K.; Zheng, L.-M.; Breedlove, B. K.; Yamashita, M. *Inorg. Chem.* **2013**, *52*, 8342.

(5) (a) Rinehart, J. D.; Long, J. R. *Chem. Sci.* **2011**, *2*, 2078. (b) Jiang, S.-D.; Liu, S.-S.; Zhou, L.-N.; Wang, B.-W.; Wang, Z.-M.; Gao, S. *Inorg. Chem.* **2012**, *51*, 3079. (c) Jiang, S.-D.; Wang, B.-W.; Sun, H.-L.; Wang, Z.-M.; Gao, S. *J. Am. Chem. Soc.* **2011**, *133*, 4730. (d) Jeletic, M.; Lin, P.-H.; Le Roy, J. J.; Korobkov, I.; Gorelsky, S. I.; Murugesu, M. *J. Am. Chem. Soc.* **2011**, *133*, 19286. (e) Yamashita, A.; Watanabe, A.; Akine, S.; Nabeshima, T.; Nakano, M.; Yamamura, T.; Kajiwara, T. *Angew. Chem., Int. Ed.* **2011**, *50*, 4016. (f) Gao, F.; Yao, M.-X.; Li, Y.-Y.; Li, Y.-Z.; Song, Y.; Zuo, J.-L. *Inorg. Chem.* **2013**, *52*, 6407. (g) Yao, M.-X.; Zheng, Q.; Gao, F.; Li, Y.-Z.; Song, Y.; Zuo, J.-L. *Dalton Trans.* **2012**, *41*, 13682. (h) Gao, F.; Cui, L.; Liu, W.; Hu, L.; Zhong, Y.-W.; Li, Y.-Z.; Zuo, J.-L. *Inorg. Chem.* **2013**, *52*, 11164. (i) Boulon, M.-E.; Cucinotta, G.; Luzon, J.; Degl'Innocenti, C.; Perfetti, M.; Bernot, K.; Calvez, G.; Caneschi, A.; Sessoli, R. *Angew. Chem., Int. Ed.* **2013**, *52*, 350. (j) Baldoví, J. J.; Cardona-Serra, S.; Clemente-Juan, J. M.; Coronado, E.; Gaita-Ariño, A.; Palii, A. *Inorg. Chem.* **2012**, *51*, 12565.

(6) (a) Karotsis, G.; Evangelisti, M.; Dalgarno, S. J.; Brechin, E. K. *Angew. Chem., Int. Ed.* **2009**, *48*, 9928. (b) Sanz, S.; McIntosh, R. D.; Beavers, C. M.; Teat, S. J.; Evangelisti, M.; Brechin, E. K.; Dalgarno, S. J. *Chem. Commun.* **2012**, *48*, 1449. (c) Karotsis, G.; Kennedy, S.; Teat, S. J.; Beavers, C. M.; Fowler, D. A.; Morales, J. J.; Evangelisti, M.; Dalgarno, S. J.; Brechin, E. K. *J. Am. Chem. Soc.* **2010**, *132*, 12983. (d) Taylor, S. M.; Karotsis, G.; McIntosh, R. D.; Kennedy, S.; Teat, S. J.; Beavers, C. M.; Wernsdorfer, W.; Piligkos, S.; Dalgarno, S. J.; Brechin, E. K. *Chem.—Eur. J.* **2011**, *17*, 7521. (e) Atwood, J. L.; Barbour, L. J.; Hardie, M. J.; Raston, C. L. *Coord. Chem. Rev.* **2001**, *222*, 3.

(7) (a) Bi, Y.-F.; Wang, X.-T.; Liao, W.-P.; Deng, R.-P.; Zhang, H.-J.; Gao, S. *Inorg. Chem.* **2009**, *48*, 11743. (b) Tan, H.-Q.; Du, S.-C.; Bi, Y.-F.; Liao, W.-P. *Chem. Commun.* **2013**, *49*, 8211. (c) Liu, M.; Liao, W.-P.; Hu, C.-H.; Du, S.-C.; Zhang, H.-J. *Angew. Chem., Int. Ed.* **2012**, *51*, 1585. (d) Liu, C.-M.; Zhang, D.-Q.; Hao, X.; Zhu, D.-B. *Cryst. Growth Des.* **2012**, *12*, 2948. (e) Su, K.-Z.; Jiang, F.-L.; Qian, J.-J.; Wu, M.-Y.; Xiong, K.-C.; Gai, Y.-L.; Hong, M.-C. *Inorg. Chem.* **2013**, *52*, 3780.

(8) Arduini, A.; Casnati, A. *Macrocycle Synthesis*; Parker, O., Ed.; Oxford University Press: New York, 1996; Chapter. 7.

(9) Kläui, W.; Muller, A.; Eberspach, W.; Boese, R.; Goldbergs, I. *J. Am. Chem. Soc.* **1987**, *109*, 164.

(10) *SAINT-Plus, version 6.02*; Bruker Analytical X-ray System: Madison, WI, 1999.

(11) Sheldrick, G. M. *SADABS An Empirical Absorption Correction Program*; Bruker Analytical X-ray Systems: Madison, WI, 1996.

(12) Sheldrick, G. M. *SHELXTL-97*; Universität of Göttingen: Göttingen, Germany, 1997.

(13) Boudreaux, E. A.; Mulay, L. N. *Theory and Application of Molecular Paramagnetism*; John Wiley & Sons: New York, 1976; p 491.

(14) (a) Abbas, G.; Lan, Y. H.; Kostakis, G. E.; Wernsdorfer, W.; Anson, C. E.; Powell, A. K. *Inorg. Chem.* **2010**, *49*, 8067. (b) Ke, H.-S.; Xu, G.-F.; Guo, Y.-N.; Gamez, P.; Beavers, C. M.; Teat, S. J.; Tang, J.-K. *Chem. Commun.* **2010**, *46*, 6057.

(15) (a) Osa, S.; Kido, T.; Matsumoto, N.; Re, N.; Pochaba, A.; Mrozinski, J. *J. Am. Chem. Soc.* **2004**, *126*, 420. (b) Bi, Y.; Guo, Y.-N.; Zhao, L.; Guo, Y.; Lin, S.-Y.; Jiang, S.-D.; Tang, J.-K.; Wang, B.-W.; Gao, S. *Chem.—Eur. J.* **2011**, *17*, 12476.

(16) Tang, J.-K.; Hewitt, I.; Madhu, N. T.; Chastanet, G.; Wernsdorfer, W.; Anson, C. E.; Benelli, C.; Sessoli, R.; Powell, A. K. *Angew. Chem., Int. Ed.* **2006**, *45*, 1729.

(17) (a) Ren, M.; Bao, S.-S.; Hoshino, N.; Akutagawa, T.; Wang, B.-W.; Ding, Y.-C.; Wei, S.-Q.; Zheng, L.-M. *Chem.—Eur. J.* **2013**, *19*, 9619. (b) Wernsdorfer, W. *C. R. Chim.* **2008**, *11*, 1086.

(18) Katoh, K.; Horii, Y.; Yasuda, N.; Wernsdorfer, W.; Toriumi, K.; Breedlove, B. K.; Yamashita, M. *Dalton Trans.* **2012**, *41*, 13582.

(19) Sugita, M.; Ishikawa, N.; Ishikawa, T.; Koshihara, S.; Kaizu, Y. *Inorg. Chem.* **2006**, *45*, 1299.

(20) (a) Katoh, K.; Kajiwara, T.; Nakano, M.; Nakazawa, Y.; Wernsdorfer, W.; Ishikawa, N.; Breedlove, B. K.; Yamashita, M. *Chem.—Eur. J.* **2011**, *17*, 117. (b) Cole, K. S.; Cole, R. H. *J. Chem. Phys.* **1941**, *9*, 341.